Mesoscale variability of sea surface pCO_2: What does it respond to?

A. Mahadevan
Department of Earth Sciences, Boston University, Boston, Massachusetts, USA

M. Lévy and L. Mémery[1]
Laboratoire d'Océanographie Dynamique et de Climatologie, CNRS/IRD/UPMC, Paris, France

Received 29 May 2003; revised 21 October 2003; accepted 19 November 2003; published 30 January 2004.

[1] We examine the impact of mesoscale and submesoscale oceanic processes on the distribution of sea surface pCO_2 to explain variability observed at length scales of order 10 km. We ask whether the large pCO_2 excursions (50–150 μ-atm) that occur over 10–25 km of the sea surface could be induced by vertical advection associated with fronts and eddies in the pelagic ocean. A numerical model of a highly resolved, but idealized, mesoscale flow field is used to model the surface pCO_2 response to submesoscale upwelling, taking into account the effect of wind, heat flux, and phytoplankton production. The effect of upwelled DIC on surface pCO_2 is largely offset by the lower temperature of the upwelled water and the consumption of DIC by phytoplankton that respond to the simultaneously upwelled nitrate in a nutrient-limited setting. Since an upwelling-induced change in surface temperature, DIC, or nitrate is proportional to the vertical gradient of these properties beneath the mixed layer, the relative change in surface pCO_2 is also dependent on the relative strengths of these gradients. We find that only small variations in surface pCO_2 (∼10 μ-atm) are induced by submesoscale upwelling. The larger (50–150 μ atm) variations observed at small scales (∼10 km) are therefore not a direct consequence of submesoscale upwelling. Our results suggest that these surface pCO_2 differences are likely to have been generated at larger scales (by differential properties and levels of biological productivity) and cascaded to smaller scales by horizontal advection at the sea surface. *INDEX TERMS:* 4572 Oceanography: Physical: Upper ocean processes; 4825 Oceanography: Biological and Chemical: Geochemistry; 4806 Oceanography: Biological and Chemical: Carbon cycling; 4842 Oceanography: Biological and Chemical: Modeling; *KEYWORDS:* mesoscale, pCO_2, variability

Citation: Mahadevan, A., M. Lévy, and L. Mémery (2004), Mesoscale variability of sea surface pCO_2: What does it respond to?, *Global Biogeochem. Cycles*, *18*, GB1017, doi:10.1029/2003GB002102.

1. Introduction

[2] The exchange of carbon dioxide (CO_2) between the atmosphere and ocean is driven by a difference in the partial pressures of CO_2 (pCO_2) across the air-sea interface. The gas flux depends largely on the magnitude of the partial pressure difference and the wind intensity. While atmospheric pCO_2 is fairly uniform and well-monitored, oceanic pCO_2 is variable in space and time, and poorly sampled. Present-day global estimates of the air-sea CO_2 flux are based on a compilation of sea surface pCO_2 measurements into mean climatological monthly maps [*Takahashi et al.*, 1997; *Takahashi*, 2002; *Feely et al.*, 2002] that are used along with estimated wind speeds and an exchange coefficient formulation [*Wanninkhof*, 1992], to calculate monthly climatological air-sea fluxes of CO_2 at a global resolution of $4° \times 5°$. While these estimates have brought us a long way in our search for a better quantification of the sources and sinks for atmospheric CO_2, there are still several questions and concerns about neglecting the smaller-scale variability in the pCO_2 and wind fields and the errors that might result as a consequence. Since pCO_2 is a nonlinear function of several variables, its value computed from a regional mean of the variables could be somewhat different than the mean regional pCO_2 [*Trela et al.*, 1995]. It is not clear whether sea surface pCO_2 is normally distributed and whether the climatological distributions of pCO_2 constructed by compositing several years of data appropriately represent the mean. Since the net global flux of carbon into the ocean is the small difference between a large in- and out-flux, it is sensitive to variability in either component. We thus have an interest in understanding and resolving the high degree of

[1]Now at Laboratoire des Sciences de l'Environnement Marin (LEMAR), Institut Universitaire Européen de la Mer (IUEM), CNRS/UBO, Plouzané, France.

0886-6236/04/2003GB002102$12.00

spatial and temporal variability occurring in surface pCO_2 and the resulting air-sea flux of CO_2.

[3] It is known that surface pCO_2 can show significant seasonal [*Takahashi et al.*, 1993; *Bates et al.*, 1998; *Metzl et al.*, 1995], as well as interannual [*Bates*, 2002; *Feely et al.*, 1999; *Lefèvre et al.*, 1999] variability. But variability is also observed on shorter timescales ranging from days to weeks [*Taylor et al.*, 1992; *Hood et al.*, 1999, 2001] that are associated with meso (10–100 km) and submeso (1–10 km) length scale dynamics in the ocean. *Bates et al.* [2000] observe a spectral peak in the variability of sea surface pCO_2 and its temperature-adjusted value at mesoscales, suggesting that its variability is largely coupled to the dynamics. *Watson et al.* [1991] observed that in the late spring and early summer, sea surface pCO_2 in the North Atlantic was strongly modulated by biological activity, and that pCO_2, as well as the total dissolved inorganic carbon (DIC), were negatively correlated with chlorophyll. Variations of 5–10 μ-atm across 10 km were common, but even variations as large as 70 μ-atm were found to occur across tens of kilometers. In the Indian Ocean, N. Metzl et al. (personal communication, 2002) observed pCO_2 excursions of ~150 μ-atm over tens of kilometers during the early summer. Here too, the DIC was strongly modulated by biology and showed strong anti-correlation with fluorescence. The Carioca buoy and POMME data (N. R. Bates et al., personal communication, 2002) from the North Atlantic are rife with smaller variations overlaid, sometimes, on a gradual trend. In these data sets, both temperature and DIC are seen to exert the dominant control on pCO_2 in different instances. A gradual increase in temperature is reflected in a corresponding rise the pCO_2, while large and abrupt DIC variations that result from phytoplankton blooms generate more dramatic pCO_2 variations.

[4] This work is aimed at improving our understanding of the mesoscale and submesoscale variability of pCO_2 and its controlling processes. It is motivated by the need to understand observations such as those described above. In particular, we aim to assess the role of mesoscale ocean dynamics on the sea surface pCO_2 variability. During spring bloom conditions, the vertical gradients of DIC, NO_3 and temperature are relatively weak or nonexistent in the upper ocean. DIC, NO_3, and temperature are poorly correlated, nutrients are available at the surface, and the local consumption of DIC by phytoplankton can drive large pCO_2 variations. The large horizontal variability in pCO_2 that is generated in such situations is likely to cascade to smaller scales due to stirring by horizontal advection, as is shown for phytoplankton [*Abraham*, 1998; *Lévy*, 2003]. During oligotrophic conditions, on the other hand, the surface waters are generally depleted of nutrients, convective mixing is minimal, and there are strong vertical gradients in temperature, DIC, and NO_3 just beneath the mixed layer. Under such conditions, mesoscale and submesoscale upwelling associated with fronts and eddies in the ocean contribute significantly to the delivery of nutrients to the surface, thereby affecting the levels of new and primary production [*Lévy et al.*, 2001; *Mahadevan and Archer*, 2000; *McGillicuddy et al.*, 1998; *Flierl and McGillicuddy*, 2002; *Follows and Williams*, 2003, and references therein]. Such upwelling can occur at scales smaller than the characteristic eddy scale (the internal Rossby radius of deformation) and hence introduce small-scale variance in the surface distributions [*Mahadevan and Campbell*, 2002]. It can significantly modulate not only the nutrients and biology in the surface ocean, but also temperature and DIC. The potential implications of these vertical fluxes on surface pCO_2 raises several questions. What magnitude of pCO_2 variations can potentially be induced by the dynamics? To what parameters are these variations most sensitive? Is mesoscale and submesoscale vertical transport the major cause of surface pCO_2 variability and can it account for the large pCO_2 excursions that are observed over tens of kilometers? These are the sorts of issues that we intend to address through this study.

[5] The pCO_2 of seawater varies largely with the temperature, T, of the water, its DIC content, and total alkalinity, ALK. It increases nonlinearly with T and DIC, but decreases with ALK. In general, DIC increases with depth in the ocean, while temperature decreases with depth. Hence the upwelling of DIC from the subsurface tends to increase sea surface pCO_2, but the lower temperature of the upwelled water counters this. In addition, the biological production of phytoplankton that is induced by the upwelling of nutrients (nitrate and phosphate) consumes DIC in the surface layer and draws down surface pCO_2. The change in surface T, DIC, and ALK that is induced by upwelling is a function not only of the upwelling intensity, but also of the vertical gradients of these properties beneath the mixed layer, the mixed-layer depth, and mixing efficiency. If we assume Redfield stoichiometry, the DIC consumed by biological production at the surface is proportional to the nitrate (NO_3) upwelled, which in turn is related to the vertical gradient of the NO_3. Hence, for a given intensity of upwelling, the modulation in surface pCO_2 is dependent on the relative vertical gradients of T, DIC, ALK, and NO_3. In the long run, the cumulative rate of vertical exchange affects the vertical gradients of these tracers in the ocean, but in this study, we merely examine the effect of localized vertical transport on surface pCO_2 as a function of the vertical gradients.

[6] This study focuses on the effects of intermittent and small-scale upwelling associated with fronts and eddies, rather than the persistent large-scale upwelling that is observed, for example, in the equatorial upwelling zones. When the upwelling is associated with a large-scale wind field, the divergence of the surface layer draws water up to the surface over large areas. The deep mixed layer in the equatorial upwelling zones may also be a result of the strong shear due to the equatorial undercurrent. The net result is that the upwelled DIC makes its expression at the surface. The heat flux, that also occurs on large scales, contributes to the warming of the DIC-rich upwelled waters and results in substantially elevating the surface pCO_2. Thus the cumulative effect of heat flux and upwelling is important in the evolution of surface pCO_2 on the global scale as, for example, in the equatorial oceans. However, it is thought to be relatively less important in the case of submesoscale upwelling for reasons explained in the section describing our results.

[7] In what follows, we describe a modeling study to address the questions raised by observations of sea surface

pCO_2. We use a high-resolution three-dimensional ocean circulation model to simulate the dynamics of a meandering front with eddies and the associated vertical transport. A state of the art ecological model consisting of interactions between nitrate, phytoplankton, zooplankton, ammonia, detritus, and dissolved organic matter is used to simulate the biological response in the upper ocean and its effect on the carbon and nitrogen chemistry of the water. We also model the mixed layer dynamics of the upper ocean which is forced with wind and heat fluxes. We initialize the T, DIC, and NO_3 fields in the model based on commonly found values for the vertical gradients of these properties in the North Atlantic subtropical gyre. The sensitivity of the surface pCO_2 to upwelling depends on the ratios of the vertical gradients of T, DIC, and NO_3.

2. Modeling

2.1. Model Configuration

[8] We use the OPA primitive equation ocean model from LODYC [*Madec et al.*, 1999] to simulate interactive mesoscale structures resulting from the nonlinear evolution of an unstable baroclinic front. Fronts are ubiquitous to the ocean, and their meanders often develop into eddies, as is seen in our simulation. Hence we consider the evolving front and its associated structures to be a general representation of an energetic mesoscale flow field in the ocean. The model is set up in a channel-like domain 162 km in east-west extent, 486 km in north-south extent, and 4000 m deep, with solid north-south boundaries and periodic east-west boundaries. We treat density as a function of temperature alone; the salinity is uniform and constant. The upper layers of the southern half of the channel are warmer than the northern half, and the mid-channel density is an interpolation of the northern and southern density profiles. The basic state is an east-west uniform potential vorticity zonal jet in geostrophic and hydrostatic balance. The jet-like flow is aligned with the contours of density on account of geostrophy. The mean density profile yields a first baroclinic Rossby radius of deformation of approximately 30 km. Details of the model and a physical description of the flow are given by *Lévy et al.* [2001]. We use a model resolution of 2 km $\times$ 2 km in the horizontal plane in order to resolve the submesoscale vertical velocities. In the vertical, the grid resolution varies. It is finer in the upper ocean, starting at 10 m near the surface and gradually increasing to 300 m at depth.

[9] The dynamical model is coupled to a biogeochemical model for nitrate, phytoplankton, zooplankton, ammonia, detritus, dissolved organic matter, and DIC. The DIC is coupled in Redfield proportion to NO_3, which is the limiting nutrient. The parameters for the biological model are the same as those of *Lévy et al.* [2001]. We experiment with and without the biological contribution and with different values of wind stress and net surface heat flux. Wind stress and a negative heat flux applied at the surface of the model induce mixing. The deepening of the mixed layer is also influenced by the density stratification and velocity shear. Since we are interested in mesoscale variations in sea-surface pCO_2 on a timescale of weeks and want to isolate the effect of vertical motion, we neglect the air-sea transfer of CO_2 which occurs over much longer timescales. It would take a 100-m-deep mixed layer, for example, about a year to equilibrate its pCO_2 with the atmosphere by air-sea flux.

2.2. Model Parameters

[10] The sensitivity of surface pCO_2 to mesoscale and submesoscale upwelling is largely a function of the ratio of the vertical gradients of T, DIC, ALK, and NO_3 just beneath the mixed layer. This can be seen by expressing the change in pCO_2, ΔpCO_2, in terms of the variations in T, DIC, and ALK, namely, ΔT, ΔDIC, ΔALK, as [*Takahashi et al.*, 1993]

$$\Delta \mathrm{pCO_2} = \frac{\partial \mathrm{pCO_2}}{\partial \mathrm{T}}\Delta \mathrm{T} + \frac{\partial \mathrm{pCO_2}}{\partial \mathrm{DIC}}\Delta \mathrm{DIC} + \frac{\partial \mathrm{pCO_2}}{\partial \mathrm{ALK}}\Delta \mathrm{ALK}. \quad (1)$$

The relative change in pCO_2 to temperature, expressed as $\beta \equiv \frac{1}{\mathrm{pCO_2}}\frac{\partial \mathrm{pCO_2}}{\partial T}$, is fairly constant in the ocean [*Takahashi et al.*, 1993]. Using this definition of β, the Revelle factor $\xi \equiv \frac{\Delta \mathrm{pCO_2}}{\mathrm{pCO_2}} / \frac{\Delta \mathrm{DIC}}{\mathrm{DIC}}\Big|_{\mathrm{ALK=const}}$, and its alkalinity equivalent $\xi_A \equiv \frac{\Delta \mathrm{pCO_2}}{\mathrm{pCO_2}} / \frac{\Delta \mathrm{ALK}}{\mathrm{ALK}}\Big|_{\mathrm{DIC=const}}$, we can express the relative change in pCO_2 due to T, DIC, and ALK variations as

$$\frac{\Delta \mathrm{pCO_2}}{\mathrm{pCO_2}} = \beta \Delta T + \xi \frac{\Delta \mathrm{DIC}}{\mathrm{DIC}} + \xi_A \frac{\Delta \mathrm{ALK}}{\mathrm{ALK}}. \quad (2)$$

The rate of change of a property, for example T, due to advection by a vertical velocity w is given as $\frac{\partial T}{\partial t} = -w\frac{\partial T}{\partial z}$. Hence the relative change in surface pCO_2 in a time interval Δt that is caused by upwelling can be written as

$$\frac{\Delta \mathrm{pCO_2}}{\mathrm{pCO_2}} = -\frac{w\Delta t}{\Delta z}\left(\beta \Delta \mathrm{T}_z + \xi \frac{\Delta \mathrm{DIC}_z}{\mathrm{DIC}} + \xi_A \frac{\Delta \mathrm{ALK}_z}{\mathrm{ALK}}\right), \quad (3)$$

where ΔT_z, ΔDIC_z, and ΔALK_z are the vertical variations in T, DIC, and ALK occurring over a height Δz just beneath the mixed layer. By denoting the ratios of the second and third terms in parenthesis to the first as

$$\gamma_C \equiv \frac{-\xi}{\beta \mathrm{DIC}}\frac{\Delta \mathrm{DIC}_z}{\Delta \mathrm{T}_z} \quad \text{and} \quad \gamma_A \equiv \frac{-\xi_A}{\beta \mathrm{ALK}}\frac{\Delta \mathrm{ALK}_z}{\Delta \mathrm{T}_z}, \quad (4)$$

and taking ΔT_z to be non-zero below the mixed layer, the relative change in pCO_2 due to upwelling can be expressed as

$$\frac{\Delta \mathrm{pCO_2}}{\mathrm{pCO_2}} = -\frac{w\Delta t}{\Delta z}(1-\gamma)\beta \Delta_z \mathrm{T}, \quad \text{where} \quad \gamma = \gamma_C + \gamma_A. \quad (5)$$

[11] In most regions of the ocean, the vertical gradients of ALK are weak as compared to those of DIC, i.e., $|\gamma_A| < |\gamma_C|$. Alkalinity and salinity are held constant in this model for simplicity and effectively $\gamma = \gamma_C$. Alternatively, the DIC in the model can be interpreted as a combination of the DIC and ALK in the ocean, so that henceforth we use only one parameter γ (rather than γ_C and γ_A) and one variable, namely, DIC (instead of DIC and ALK). Temperature and DIC are generally negatively correlated in the ocean, so that $\Delta DIC_z/\Delta T_z < 0$ and $\gamma > 0$. If $\gamma = 1$, it means that upwelling

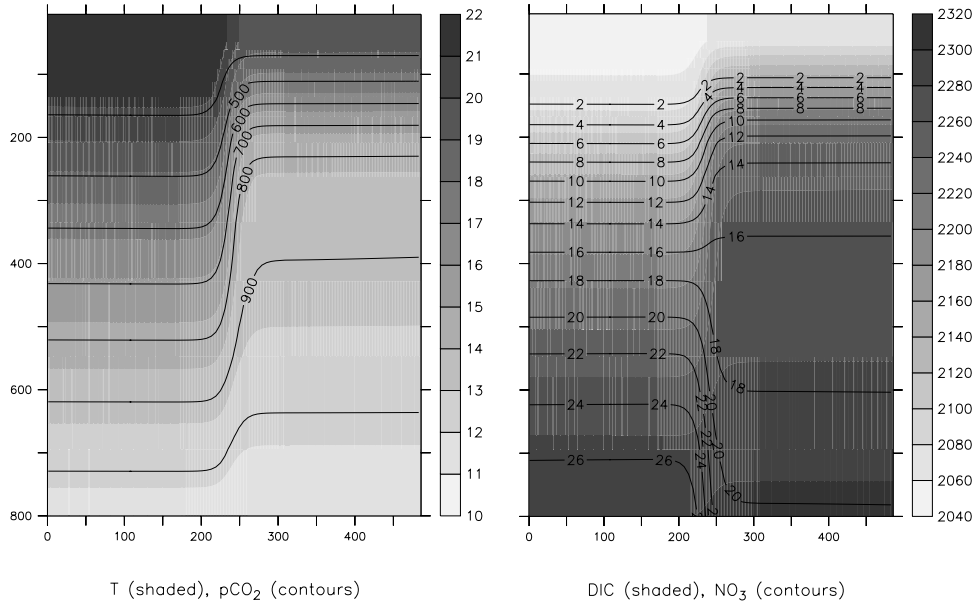

Figure 1. Initial distributions of T, DIC, NO_3, and pCO_2 along a mid-channel north-south cross-section that shows the upper 800 m of the domain. The pCO_2 is evaluated at atmospheric pressure. The horizontal axis is labeled in kilometers and vertical axis in meters. The north-south boundaries are impervious. In this initialization, we used $\gamma = 4$, $\gamma_s = 1$, and $\delta = 0.75$, which results in $\Gamma = 1$. The north-south NO_3 gradient reverses sign at depth because the vertical gradients are weak at depth on the north side of the channel. The profiles of DIC, T, and NO_3 are representative of the ocean in the upper 500 m; the distributions at depth are hardly of relevance to the model results.

has no effect on surface pCO_2, because the effect of DIC and temperature cancel each other. If, on the other hand, $\gamma > 1$, the surface pCO_2 is increased by upwelling, and if $\gamma < 1$, the pCO_2 is decreased by upwelling. This is the case when no biological consumption of DIC is considered.

[12] In a nutrient limited setting, the DIC consumed by phytoplankton in a time interval Δt in response to a submesoscale upwelling velocity w is denoted by Δ_{bio}DIC and estimated as the upwelled NO_3 times the Redfield ratio $R_{C:N}$, i.e., $-\frac{w\Delta t}{\Delta z}\,\Delta NO_{3z} R_{C:N}$, where $NO_{3z}/\Delta z$ is the vertical gradient of nitrate beneath the mixed layer. Expressing the ratio of the DIC consumed by phytoplankton to the upwelled DIC as

$$\delta = R_{C:N}\,\frac{\Delta NO_{3z}}{\Delta DIC_z}, \tag{6}$$

we can express the biological uptake of DIC resulting from the vertical nitrate flux as

$$\Delta_{bio}DIC = -\frac{w\Delta t}{\Delta z}\,\delta\,\Delta DIC_z. \tag{7}$$

This must be deducted from the upwelled DIC, resulting in the relative change in pCO_2 to be modified as

$$\frac{\Delta pCO_2}{pCO_2} = -\frac{w\Delta t}{\Delta z}(1-\Gamma)\beta\Delta T_z, \quad \text{where} \quad \Gamma = \gamma(1-\delta). \tag{8}$$

The parameter Γ takes into account the effect of biological productivity. When $\Gamma = 1$, vertical transport has no net effect on the surface pCO_2 after accounting for biological consumption, but when $\Gamma > 1$ or <1, one can expect localized upwelling to increase, or respectively, decrease surface pCO_2.

2.3. Model Initialization

[13] We initialize the model domain with an across-channel front in temperature (Figure 1) as in the work by *Lévy et al.* [2001]. To initialize the DIC, we choose a value for γ to characterize the correlation between DIC and T in the vertical. An analogous parameter γ_s is used to relate DIC and T at the sea surface. The idea is that by setting $\gamma_s = 1$, the sea surface pCO_2 can be made uniform even when $\gamma \neq 1$. Further, the relationship between DIC and T is likely to be different at the sea surface than at depth because of air-sea gas exchange, heat fluxes, and biological activity. To initialize the model DIC as a function of the T field, we prescribe a value of DIC at any one point in the surface layer of the model. The DIC at any neighboring location varies from the initial location by $\Delta DIC = -\beta DIC\ \gamma^*\ \Delta T/\xi$ in accordance with equation (4), where ΔT is the temperature variation between the two locations and ξ is evaluated at the new location. The parameter γ^* takes the value γ_s at the surface, but changes to γ at depth to generate vertical gradients in the desired ratio. It is evaluated as $\gamma^* = \gamma_s \exp(-z/z_m) + \gamma\,(1 - \exp(-z/z_m))$, where z is the depth below the mixed layer, and z_m is taken to be 50 m. Using such a blending function ensures that the DIC varies smoothly on isopycnals that are exposed to the surface on one side of the front, but lie subsurface and have a different DIC value on the other side. Choosing γ_s, γ, and the value of DIC at any one point at the surface thus defines the DIC distribution in terms of T over the entire domain. The initial T and DIC

fields are shown in Figure 1 when $\gamma_s = 1$ and $\gamma = 4$. When $\gamma_s = 1$, the meridional change in T at the surface is compensated by the change in DIC; this is representative of a situation in which the sea surface pCO_2 is perfectly equilibrated with the atmosphere. We use $\gamma_s = 1$ to isolate the effect of vertical advection on surface pCO_2 from that of horizontal advection. Using coarsely gridded global estimates of the mean climatological DIC, ALK, and T distributions, we estimated the value γ for the world's oceans (manuscript in preparation). It was found that γ lies in the range 1–2 for about 50% of the world's oceans, 2–3 for 15–20% of the ocean, and 3–5 for 5–10% of the ocean. We take γ to be 4 to simulate conditions in which the surface pCO_2 is sensitive to upwelling.

[14] In the model runs with biology, we need to initialize the nitrate field. We set the initial NO_3 concentration to 0 above the nutricline, which we set at 100 m to mimic summer-like conditions in which productivity is limited by the vertical advective supply of nutrients occurring at submesoscales. Beneath the nutricline, we relate NO_3 to DIC by choosing a value of δ and thereby prescribing the vertical NO_3 gradient in accordance with equation (6). $R_{C:N}$ is taken to be 6.625. We run each model simulation with the same initial temperature and velocity fields, but can vary the initial DIC and NO_3 distributions by changing γ, γ_s and δ.

2.4. Numerics

[15] All the variables in the model, T, DIC, NO_3, phytoplankton, zooplankton, ammonia, detritus, and dissolved organic matter, are advected by the flow field. We find that spurious values of pCO_2 can be generated by using different numerical advection algorithms (or different time steps, eddy viscosity coefficients, or convective adjustment) for DIC and T, the variables on which pCO_2 is dependent. Since the distributions of DIC and T are negatively correlated, i.e., an increase in one is generally associated with a decrease in the other, and pCO_2 increases nonlinearly with each of them, a discrepancy in the rates of propagation of DIC and T can lead to exceptionally large excursions in pCO_2. This particularly stands out at the frontal outcrop when the domain is initialized with large but negatively correlated variations in DIC and T across the front that generate a uniform pCO_2 field throughout the domain ($\gamma = \gamma_s = 1$). To avoid such errors, we have used the same numerics for all the variables. Since the Arakawa scheme is used for the advection of temperature [*Madec et al.*, 1999], we use the same for all the other variables.

3. Results

3.1. Dynamical Processes

[16] The model is started from a geostrophically balanced state. The front that separates warm surface water in the southern half of the channel from cooler water in the north is associated with an east-west jet in the upper ocean. The front is baroclinically unstable, and the weak initial meander introduced as a perturbation to the front grows as the simulation progresses. The meandering grows until eddies are pinched off, and the across-front mixing caused in this way leads to the gradual decay of the front. Results shown and discussed here are only for the first month of the simulation which entails meander growth and eddy pinch-off. The general evolution of the sea surface temperature (SST) pattern is for this period is shown in Figure 2.

[17] Deviations from geostrophic balance arising, for example, from the growth of instabilities can lead to non-divergent horizontal velocities and to upwelling and subduction that occurs largely along sloping isopycnal surfaces. These vertical velocities occur in narrow regions and are closely associated with strong vorticity gradients characteristic of frontogenesis [*Woods*, 1988; *Pollard and Regier*, 1992; *Shearman et al.*, 1999]. The magnitude of the vertical velocities is sensitive to the horizontal spatial resolution in the numerical model. Resolving the strong vorticity gradients and the associated dynamics at the filament scale is essential for capturing the vertical transport correctly [*Lévy et al.*, 2001]. Water that is upwelled isopycnally to the base of the mixed layer is then conveyed to the surface by vertical mixing that is induced by buoyancy and momentum fluxes at the surface. Sea surface DIC and pCO_2 are therefore sensitive to the intensity of mixing and hence to the intensity and intermittency of the wind stress [*Bates and Merlivat*, 2001; *Mémery et al.*, 2002]. Our model simulations generate upwelling advective velocities in the range of 10–50 m per day at an approximate depth of 100 m [*Lévy et al.*, 2001]. This is typical of fairly energetic eddies and fronts in the ocean. We impose a uniform surface wind stress of 0.3 dyn cm^{-2} to induce a reasonable level of mixing and maintain an average mixed layer depth of about 60 m. Without this wind-induced mixing, the signal of upwelling is not detectable at the surface. Figure 3 shows a vertical across-front section through the upper 120 m of the model domain. The dynamical uplift of DIC and cold water is seen in the upper thermocline, while the effect of vertical mixing in conveying these signals to the surface is seen in the upper 50 m or so. NO_3 is also uplifted into the euphotic layer along with DIC and a maximum in phytoplankton is generated at a depth of 40–50 m where light and nutrients are best optimized.

3.2. Competing Effects of Vertical Advection on Surface T and DIC

[18] When the model is initialized with uniform pCO_2 in the surface mixed layer ($\gamma_s = 1$), variations in surface pCO_2 can be attributed to upwelling. The magnitude of the pCO_2 variations is dependent on the value of γ in the absence of biological production and heat flux. When $\gamma = 1$, the effect of T and DIC variations induced by upwelling compensate each other, and the surface pCO_2 remains unchanged. As γ is increased in the model, one detects a greater increase in surface pCO_2 with time in regions where upwelling enhances the DIC. Figure 4b shows the surface pCO_2 after 1 month, in a model simulation performed without phytoplankton and initialized with $\gamma = 4$ and $\gamma_s = 1$. The pCO_2 is enhanced by approximately 10 μ-atm in narrow regions that occupy a small percentage of the total surface area. These conditions in the model, namely, reasonably strong vertical velocities, an active mixed layer, and a value of γ that is large compared to most of the oceans, favor the enhancement of surface pCO_2 by upwelling. An enhancement in these conditions can increase the observed variation in

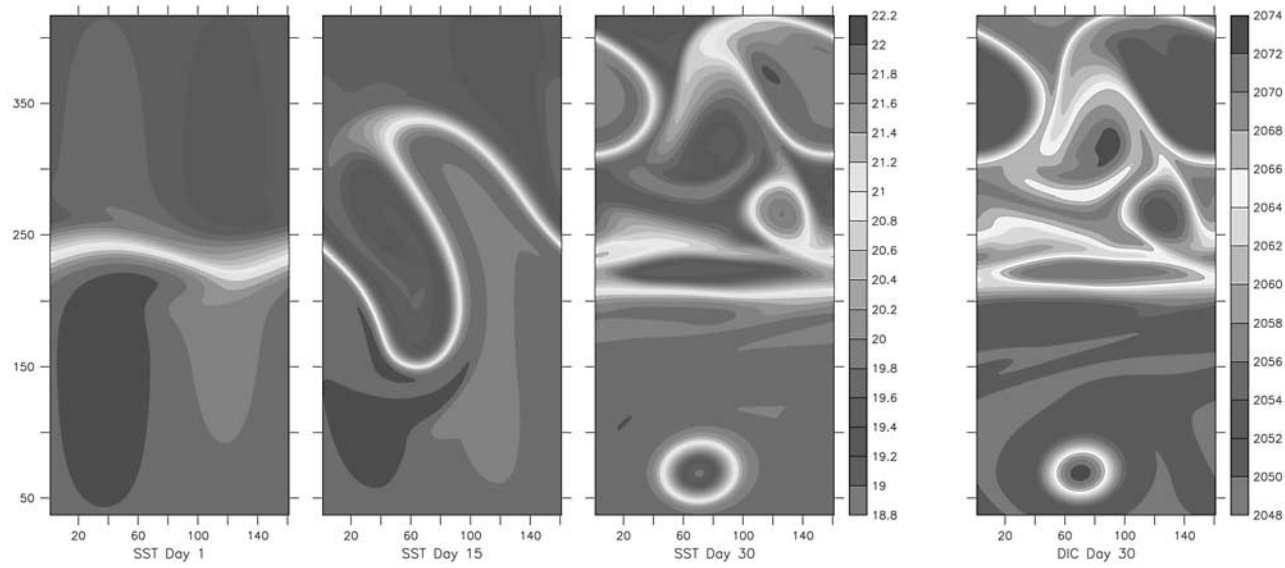

Figure 2. The first three plots show consecutive views of the model sea surface temperature and show the development of the front and mesoscale structures over a month. The last plot shows the surface DIC on day 30 of the simulation; it was initialized with $\gamma_s = 1$ and is negatively correlated with temperature. The lateral boundaries are vertical; north-south boundaries are impervious, while east-west boundaries are periodic. An east-west wind stress of 0.3 dyn cm^{-2} is imposed at the surface in this simulation. No net heat flux is prescribed here. The axes are labeled in kilometers. With an east-west wind stress, up- and down-welling is generated near the north and south boundaries. These regions are eliminated from these and all other plots. See color version of this figure at back of this issue.

surface pCO_2, but only by a factor of 2 or 3. An increased wind stress of 1 dyn cm^{-2}, for example, further increases the surface pCO_2 maxima shown in Figure 4b by about 10 μ-atm. The magnitude of pCO_2 variations generated by submesoscale upwelling seems to remain in the range of 10–20 μ-atm for the experiments without biology.

3.3. Effect of Surface Heat Fluxes

[19] When warmed, surface water becomes buoyant and isolated from the subsurface due to its strengthened stratification. This inhibits vertical mixing; the heat flux is distributed over a small depth, and surface pCO_2 can rise rapidly and substantially. In the idealized configuration of our model, the upwelled waters do not reach the surface during such times, and the subsurface DIC gradient and value of γ have little effect on the change in sea surface pCO_2. Small-scale spatial variability in pCO_2 is obliterated since the warming is large scale and not restricted to the upwelling sites. In the model, we account for only the radiative heat flux, but neglect the latent and sensible heat fluxes. The surface temperature increases by an amount proportional to the heat flux and inversely proportional to the depth of heating. The change in temperature ΔT induced by a heat flux Q in the mixed layer over a time interval Δt can be quantified as $\Delta T = Q\Delta t/C_pH$, where C_p is the specific heat capacity of the water and H is the mixed layer depth. The relative change in pCO_2 due to a heat flux (HF) can be written as $\frac{\Delta pCO_2}{pCO_2}|_{HF} = \beta\ Q\Delta t/C_pH$ and its ratio to the term in equation (3) that quantifies the relative change in pCO_2 due to the effect of upwelling on temperature is $Q/C_pHw(\Delta T_z/\Delta z)$. The variability in the heat flux Q is negligible at mesoscales and C_p is nearly constant. However, w, H and $\Delta T_z/\Delta z$ can vary at these scales. At the locations where submesoscale upwelling occurs, w is much larger than in surrounding regions, and hence the relative effect of heat flux, as compared to upwelling, is smaller at the upwelling locations than in the surrounding waters. For these reasons, the effect of surface warming in conjunction with upwelling of DIC is relatively insignificant in our model simulations of submesoscale upwelling. We see no significant further enhancement in pCO_2 by heat fluxes at the upwelling locations, as is known to occur in regions of large-scale upwelling. It is not clear whether this is entirely true in the oceans or whether the model's finding is affected by its limitations in handling the heat fluxes, mixed layer dynamics, and air-sea interaction.

[20] Cooling destabilizes and mixes the water column, resulting in the deepening of the mixed layer by entrainment, and a loss of heat over the depth of the mixed layer. Regions where the mixed layer deepens rapidly experience relatively less change in sea surface pCO_2 due to the temperature effect, as compared to regions where the cooling is restricted to a small depth. The depth of the mixed layer in the model shows considerable variability on mesoscales, as in other studies [*Nurser and Zhang*, 2000; *Lévy et al.*, 2000], and the variation of surface pCO_2 induced by cooling is linked to the variability in the mixed layer structure. In the model, we observe that the mixed layer is shallowest at fronts, around eddies, and in filaments, where the isopycnals are steeply sloping. These are the regions where surface pCO_2 is lowered the most by cooling (Figure 4c). While the surface temperature decreases,

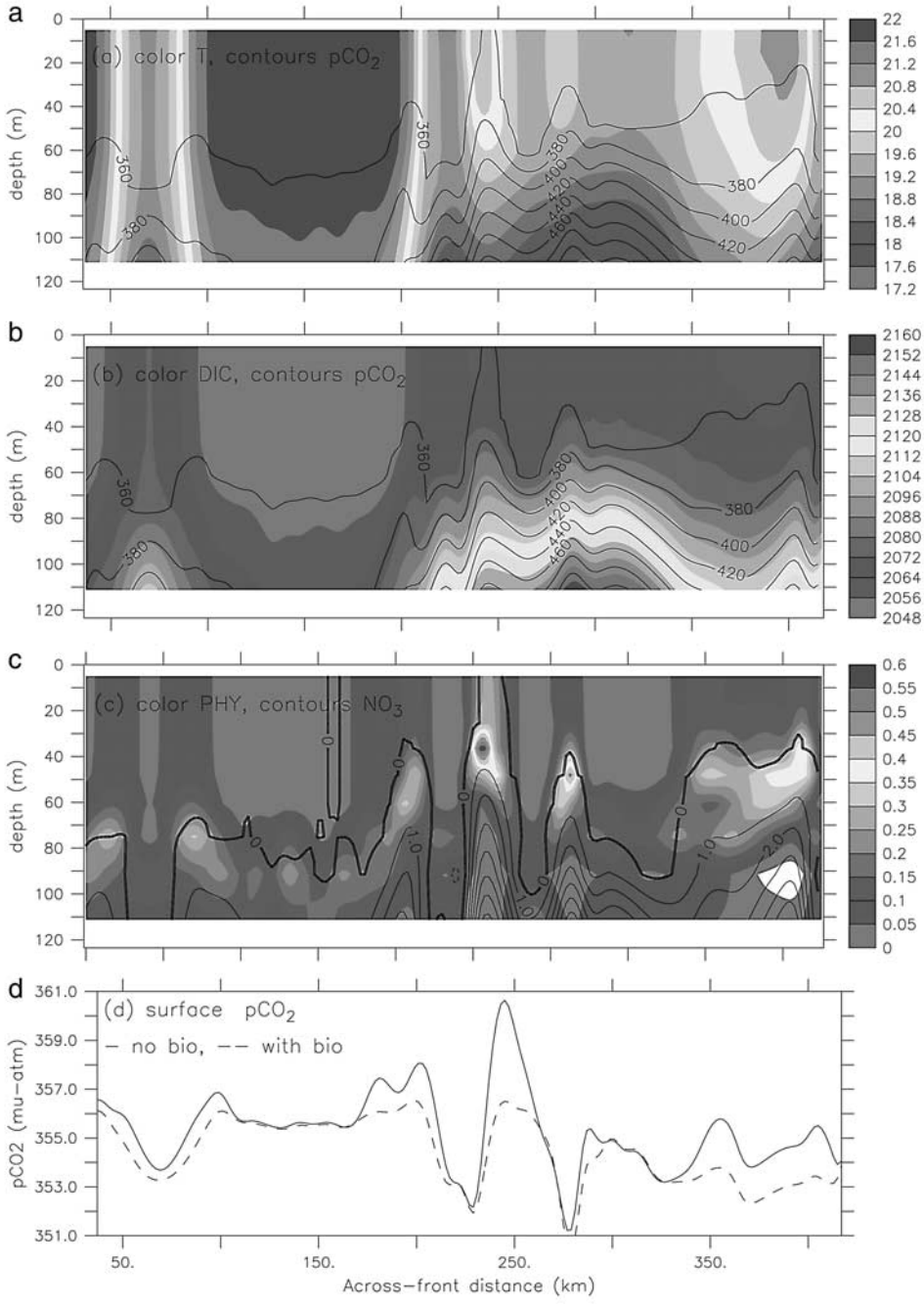

Figure 3. A north-south across-front section at x = 80 km (approximately mid-channel) showing (a) DIC and (b) temperature overlaid with contours of pCO_2 evaluated at atmospheric pressure. These fields are from day 30 of a model run initialized with $\gamma = 4$, $\gamma_s = 1$, constant ALK, and salinity, and forced with an east-west wind stress of 0.3 dyn cm^{-2}. The DIC is negatively correlated with T. There is no net heat flux and no biology in Figures 3a and 3b. DIC and cold water from the subsurface are upwelled and mixing vertically homogenizes the mixed layer conveying the upwelled water to the surface. When the wind stress is increased, the highs and lows in surface pCO_2 are more pronounced as increased mixing conveys a greater amount of upwelled DIC to the surface. (c) Phytoplankton concentration overlaid with contours of nitrate. Since nitrate is upwelled along with DIC, phytoplankton is concentrated at the sites of upwelling. It draws down the DIC and the pCO_2 as seen in Figure 3d in the regions where it had been elevated due to upwelling when there was no biology. See color version of this figure at back of this issue.

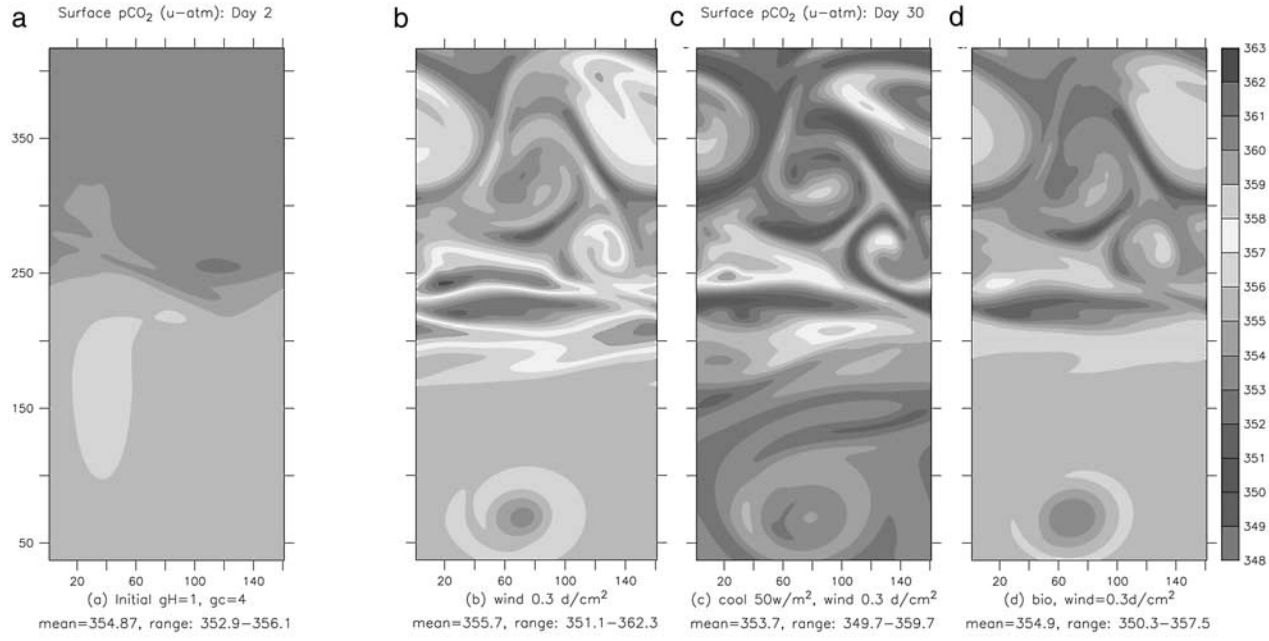

Figure 4. Surface pCO_2 in the model (a) on day 2, and (b)–(d) on day 30 of the simulation. These model runs were initialized with uniform pCO_2 at the surface and $\gamma = 4$ as shown in Figure 1. An east-west wind stress of 0.3 dyn cm^{-2} was applied at the surface. Figure 4b shows the localized increase in surface pCO_2 that results from the upwelling of DIC, though this is somewhat offset by the lowered temperature. Figure 4c shows a decrease in surface pCO_2 within certain regions when the surface is cooled by a heat loss of 50 watts m^{-2}. The reduction in pCO_2 is largest where the mixed layer depth is shallowest. Figure 4d shows the surface pCO_2 in a run with biological production that responds to the vertical flux of nitrate. The nitrate was initialized subsurface of 100 m using $\delta = 0.9$ which results in $\Gamma = 0.4$. The biological activity takes up most of the DIC upwelled and the pCO_2 enhancement seen in Figure 4b is no longer seen in Figure 4d. The range of pCO_2 variations is only 11, 10, and 7 μ-atm in each of these cases. See color version of this figure at back of this issue.

surface DIC is enhanced by the deepening of the mixed-layer and entrainment of DIC-rich water from the subsurface. The modulation of surface DIC and pCO_2 is thus dependent on the vertical DIC gradient (i.e., the value of γ) and the depth of entrainment. For a given heat loss and density distribution, higher values of γ imply a lesser drop in sea-surface pCO_2. The model simulations performed with $\gamma = 4$ and a uniform heat loss of 50 watts m^2 resulted in surface pCO_2 variations of approximately 11 μ-atm after a month. These results indicate that small-scale variability in surface pCO_2 is decreased by heating and increased by cooling.

3.4. Effect of Biology

[21] A net uptake of DIC by biological production in the upper ocean tends to lower the surface pCO_2. At times when surface waters become abundant in nutrient, phytoplankton blooms occur, and can draw down sea surface pCO_2 by as much as 50–100 μ-atm [*Taylor et al.*, 1992]. At other times, particularly in subtropical gyre centers, productivity is largely limited by the supply of nutrients. In our model simulations initialized with a nutricline at 100 m (to reflect an oligotrophic setting like that of the subtropical gyres in the late summer), new production is limited to regions where the nutrients are uplifted into the euphotic zone. This occurs in the same locations where the DIC is enhanced due to a flux from the subsurface. The uptake of DIC by phytoplankton thus curtails the enhancement of pCO_2 resulting from DIC upwelling (Figures 3d and 4d). The regions of intense upwelling are where isopycnals are sloping upward and outcropping. In the model, mixing is limited to shallow depths at such sites and the DIC modulation is visible at the surface. Under such conditions, the changes in DIC and pCO_2 are sensitive to the values of δ and Γ. For a value of $\gamma = 4$, we used $\delta = 0.6$, 0.75, and 0.9, resulting in $\Gamma = 1.6$, 1 and 0.4, respectively. These values span a large part of the range of values for δ and Γ estimated from global climatological distributions of NO_3, DIC, ALK, and T (manuscript in preparation). When $\Gamma = 1$, upwelling has little effect on surface pCO_2; when $\Gamma < 1$, surface pCO_2 is lowered by upwelling because the effects of the lowered temperature and DIC consumption outweigh the effect of upwelled DIC. Similarly, when $\Gamma > 1$, pCO_2 is increased because of a surfeit of DIC at the surface. Using a value of $\Gamma = 0.4$ (which is fairly extreme for most of the oceans and should hence maximize the variations that might be generated in surface pCO_2 by

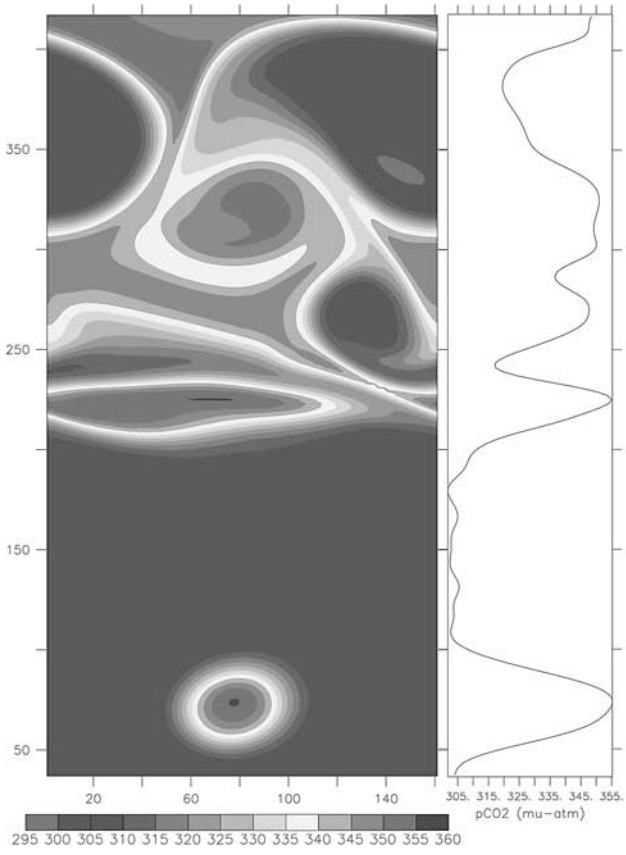

Figure 5. Surface pCO_2 on day 30 when the model is initialized with an across-front pCO_2 difference of approximately 60 μ-atm ($\gamma_s = 0.5$). The ratio of vertical DIC and T gradients is the same as in previous runs ($\gamma = 4$), but the effect of upwelling on the surface pCO_2 field is indiscernible since it is dominated by the horizontal stirring of the different pCO_2 waters. The color scale is different than in Figure 4. The variance in surface pCO_2 that initially exists at large scales is converted to smaller scales by horizontal advection as the flow evolves. The magnitude of the pCO_2 variations remains more or less unaltered. This model run was performed with a heat loss of 50 watts m^{-2}, but in general, the effect of cooling and biological productivity in response to submesoscale upwelling in undistinguishable in the surface pCO_2. The plot to the right shows the large surface pCO_2 variability along a mid-channel transect (at x = 80 km). See color version of this figure at back of this issue.

upwelling) results in localized reductions in the surface pCO_2 of only about 7 μ-atm in a month's time.

3.5. Effect of Horizontal Advection

[22] The pCO_2 of the surface ocean is much more variable than that of the atmosphere because the atmosphere is well-mixed. The surface ocean equilibrates with the atmosphere very slowly (on a timescale ~1 year) as compared to the timescales on which it is disturbed from equilibrium by upwelling, mixing, heat flux, and biological production (approximately days to weeks). It is typical to find different water masses in the surface ocean that differ in their properties, rates of biological productivity, and pCO_2. Water on one side of a front, for example, can be in greater communication with the subsurface and hence differ from the other side. If we initialize our model with a different surface pCO_2 on either side of the front ($\gamma_s \neq 1$), the evolution of the surface pCO_2 field is dominated by the lateral advection and stirring of the different pCO_2 surface waters and the impact of upwelling is indiscernible (Figure 5). This suggests that mesoscale activity influences sea surface pCO_2 not so much by submesoscale vertical transport that is crucial for nutrient supply, but rather by the horizontal advection of surface pCO_2 differences. Such pCO_2 differences are generated over larger spatial and temporal scales than those associated with submesoscale upwelling. But mesoscale and submesoscale filaments of pCO_2 variations are generated by the horizontal stirring of the different pCO_2 waters. The range of variability in surface pCO_2 values is determined by the properties and large-scale pCO_2 differences of the surface water masses that are stirred and is much larger than the variability induced by vertical fluxes alone.

4. Conclusions

[23] The variation in surface pCO_2 that can be induced by mesoscale and submesoscale vertical transport is dependent on the ratio of the vertical gradients of DIC and ALK to T (and in addition, NO_3 to DIC when biological productivity is considered, but is nutrient-limited) just beneath the mixed layer. Surface pCO_2 increases or decreases in response to submesoscale upwelling according as $\Gamma > 1$ or < 1. The magnitude of the pCO_2 modulations depend on the magnitude of $1\text{-}\Gamma$, the upwelling velocities, and the strength of wind- and cooling-induced mixing. The surface pCO_2 variations in response to submesoscale upwelling occur in frontal regions where vertical motion is pronounced. The DIC is elevated due to upwelling in such regions, but the simultaneous supply of nitrate fuels new production which consequently draws down the DIC. Warming increases sea surface pCO_2 rapidly and fairly uniformly over the region because stratification isolates the surface from below. The change in surface pCO_2 that results from cooling, on the other hand, is variable and depends on the mixed layer structure and depth of mixing, the entrainment of DIC and NO_3, and the biological consequences. Even though we initialize the DIC and NO_3 in our model to favor the response of surface pCO_2 to upwelling, we find that reasonably intense submesoscale upwelling of 10–50 m day^{-1} and fairly active mixing generated by a surface wind stress of 0.3 dyn cm^{-2}, induces surface pCO_2 variations of only about 10 μ-atm in a month's time. An increase in the mixing rate or length of simulation can somewhat increase these numbers, but they remain much smaller than the large pCO_2 variations (~100 μ-atm) that have been observed in the surface ocean over tens of kilometers. Large surface pCO_2 differences (~100 μ-atm) can occur across different water masses and fronts and when intense phytoplankton blooms draw down the DIC over certain regions, but are typically generated

over larger scales than the mesoscale and submesoscale. Our experiments suggest that the cascade of this large-scale surface pCO_2 variance to smaller scales that occurs through horizontal advection and stirring (while preserving the magnitude of the variations) is manifest as large pCO_2 excursions at small scales. The variations in surface pCO_2 generated by mesoscale and submesoscale vertical transport are much smaller ($\sim$10 μ-atm). These findings seem to be consistent with observations (e.g., *LSCOP* [2002, p.167], Carioca (N. Bates et al., personal communication, 2002), Southern Indian ocean (N. Metzl et al., personal communication, 2002)).

[24] **Acknowledgments.** This work was supported by CNRS, IDRIS, and NASA (NAG5-11258). A. M. thanks LODYC and CNRS for hosting her stay in Paris, and S. Emerson and L. Merlivat for stimulating discussions.

References

Abraham, E. (1998), The generation of plankton patchiness by turbulent stirring, *Nature*, *391*, 577–580.

Bates, N. (2002), Interannual variability in the global ocean uptake of CO_2, *Geophys. Res. Lett.*, *29*(5), 1059, doi:10.1029/2001GL013571.

Bates, N., and L. Merlivat (2001), The effect of short-term wind variability on air-sea CO_2 exchange, *Geophys. Res. Lett.*, *28*, 3281–3284.

Bates, N., T. Takahashi, D. Chipman, and A. Knap (1998), Variability of pCO_2 on diel to seasonal timescales in the Sargasso Sea, *J. Geophys. Res.*, *103*, 15,567–15,585.

Bates, N., L. Merlivat, L. Beaumont, and A. Pequignet (2000), Intercomparison of shipboard and moored CARIOCA buoy seawater fCO_2 measurements in the Sargasso Sea, *Mar. Chem.*, *72*, 239–255.

Feely, R., R. Wanninkhof, T. Takahashi, and P. Tans (1999), Influence of El Niño on the equatorial Pacific contribution to atmospheric CO_2 accumulation, *Nature*, *398*, 597–601.

Feely, R., C. Sabine, T. Takahashi, and R. Wanninkhof (2002), Uptake and storage of carbon dioxide in the ocean: The global CO_2 survey, *Oceanography*, *14*, 25–32.

Flierl, G., and D. McGillicuddy (2002), Mesocale and submesoscale physical-biological interactions in the sea, in *The Sea* (*Biological Physical Interactions in the Sea*), vol. 12, edited by A. Robinson, J. McCarthy, and B. Rotschild, pp. 113–185, John Wiley, New York.

Follows, M., and R. Williams (2003), Physical transport of nutrients and the maintenance of biological production, in *Ocean Biogeochemistry*, edited by M. Fasham, pp. 19–51, Springer-Verlag, New York.

Hood, E., L. Merlivat, and T. Johannessen (1999), Variations of fCO_2 and air-sea flux of CO_2 in the Greenland Sea gyre using high-frequency time series data from CARIOCA drift buoys, *J. Geophys. Res.*, *104*, 20,571–20,583.

Hood, E., R. Wanninkhof, and L. Merlivat (2001), Short timescale variations of fCO_2 in a North Atlantic warm-core eddy: Results from the Gas-Ex 98 carbon interface ocean atmosphere (CARIOCA) buoy data, *J. Geophys. Res.*, *106*, 2561–2572.

Lefèvre, N., A. Watson, D. Cooper, R. Weiss, T. Takahashi, and S. C. Sutherland (1999), Assessing the seasonality of the oceanic sink for CO_2 in the Northern Hemisphere, *Global Biogeochem. Cycles*, *13*, 273–286.

Lévy, M. (2003), Mesoscale variability of phytoplankton and of new production: Impact of the large-scale nutrient distribution, *J. Geophys. Res.*, *108*(C11), 3358, doi:10.1029/2002JC001577.

Lévy, M., L. Mémery, and G. Madec (2000), Combined effects of mesoscale processes and atmospheric high-frequency variability on the spring bloom in the MEDOC area, *Deep Sea Res.*, *47*, 27–53, doi:10.1016/S0967-0637(99)00,051-5.

Lévy, M., P. Klein, and A.-M. Treguier (2001), Impacts of sub-mesoscale physics on production and subduction of phytoplankton in an oligotrophic regime, *J. Mar. Res.*, *59*, 535–565.

LSCOP (2002), A Large scale CO_2 observing plan: In situ oceans and atmosphere, report, NOAA Off. of Global Programs, Silver Spring, Md.

Madec, G., P. Delecluse, and M. I. C. Levy (1999), OPA 8.1 Ocean General Circulation Model reference manual, technical report, Inst. Pierre-Simon Laplace, Paris.

Mahadevan, A., and D. Archer (2000), Modeling the impact of fronts and mesoscale circulation on the nutrient supply and biogeochemistry of the upper ocean, *J. Geophys. Res.*, *105*, 1209–1225.

Mahadevan, A., and J. Campbell (2002), Biogeochemical patchiness at the sea surface, *Geophys. Res. Lett.*, *29*(19), 1926, doi:10.1029/2001GL014116.

McGillicuddy, D., Jr., A. Robinson, D. Siegel, H. Jannasch, R. Johnson, T. Dickey, J. McNeil, A. Michaels, and A. Knap (1998), Influence of mesoscale eddies on new production in the Sargasso Sea, *Nature*, *394*, 263–266.

Mémery, L., M. Lévy, S. Vérant, and L. Merlivat (2002), The relevant time scales in estimating the air-sea CO_2 exchange in a midlatitude region, *Deep Sea Res., Part II*, *49*, 2067–2092.

Metzl, N., A. Poisson, F. Louanchi, C. Brunet, B. Schauer, and B. Bres (1995), Spatiotemporal distributions of air-sea fluxes of CO_2 in the Indian and Antarctic Oceans, *Tellus, Ser. B*, *47*, 56–69.

Nurser, A., and J. Zhang (2000), Eddy-induced mixed layer shallowing and mixed layer/thermocline exchange, *J. Geophys. Res.*, *105*, 21,851–21,868.

Pollard, R., and L. Regier (1992), Vorticity and vertical circulation at an ocean front, *J. Phys. Oceanogr.*, *22*, 609–625.

Shearman, R., J. Barth, and P. Kosro (1999), Diagnosis of three-dimensional circulation associated with mesoscale motion in the California current, *J. Phys. Oceanogr.*, *29*, 651–670.

Takahashi, T. (2002), Global sea-air CO_2 flux based on climatological surface ocean pCO_2, and seasonal biological and temperature effects, *Deep Sea Res., Part II*, *49*, 1601–1622.

Takahashi, T., J. Olafsson, J. Goddard, D. Chipman, and S. C. Sutherland (1993), Seasonal variation of CO_2 and nutrients in the high-latitude surface oceans: A comparative study, *Global Biogeochem. Cycles*, *7*, 843–878.

Takahashi, T., R. Feely, R. Weiss, R. Wanninkhoff, D. Chipman, S. Sutherland, and T. Takahashi (1997), Global air-sea flux of CO_2: An estimate based on measurements of sea-air pCO_2 difference, *Proc. Natl. Acad. Sci. U. S. A.*, *94*, 8292–8299.

Taylor, A., A. Watson, and J. E. Robertson (1992), The influence of the spring phytoplankton bloom on carbon dioxide and oxygen concentrations in the surface waters of the northeast Atlantic during 1989, *Deep Sea Res.*, *39*, 137–152.

Trela, P., S. Sathyendranath, R. Moore, and D. Kelley (1995), Effect of the nonlinearity of the carbonate system on partial pressure of carbon dioxide in the oceans, *J. Geophys. Res.*, *100*, 6829–6844.

Wanninkhof, R. (1992), Relationship between wind speed and gas exchange over the ocean, *J. Geophys. Res.*, *97*, 7373–7382.

Watson, A., C. Robinson, J. Robinson, P. Ie, B. Williams, and M. Fasham (1991), Spatial variability in the sink for atmospheric carbon dioxide in the North Atlantic, *Nature*, *350*, 50–53.

Woods, J. (1988), Mesoscale upwelling and primary production, in *Toward a Theory on Biological-Physical Interactions in the World Ocean*, edited by B. Rothschild, pp. 7–38, Kluwer Acad., Norwell, Mass.

M. Lévy, Laboratoire d'Oceanographie Dynamique et de Climatologie, Institut Pierre Simon Laplace, Universite de Paris VI, Paris France. (levy@lodyc.jussieu.fr)

A. Mahadevan, Department of Earth Sciences, Boston University, 685 Commonwealth Avenue, Boston, MA 02215, USA. (amala@bu.edu)

L. Mémery, Laboratoire des Sciences de l'Environnement Marin (LEMAR), Institut Universitaire Europen de la Mer (IUEM), Technopole Brest Iroise, Place Nicolas Copernic, 29820 Plouzan, France. (memery@univ-brest.fr)

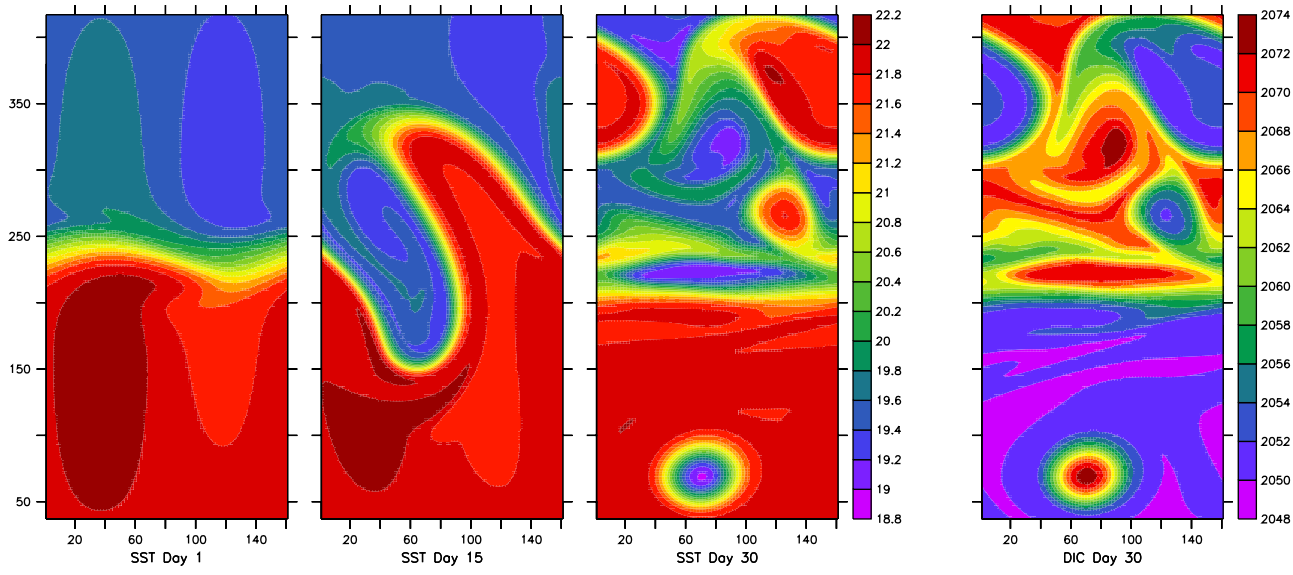

Figure 2. The first three plots show consecutive views of the model sea surface temperature and show the development of the front and mesoscale structures over a month. The last plot shows the surface DIC on day 30 of the simulation; it was initialized with $\gamma_s = 1$ and is negatively correlated with temperature. The lateral boundaries are vertical; north-south boundaries are impervious, while east-west boundaries are periodic. An east-west wind stress of 0.3 dyn cm^{-2} is imposed at the surface in this simulation. No net heat flux is prescribed here. The axes are labeled in kilometers. With an east-west wind stress, up- and down-welling is generated near the north and south boundaries. These regions are eliminated from these and all other plots.

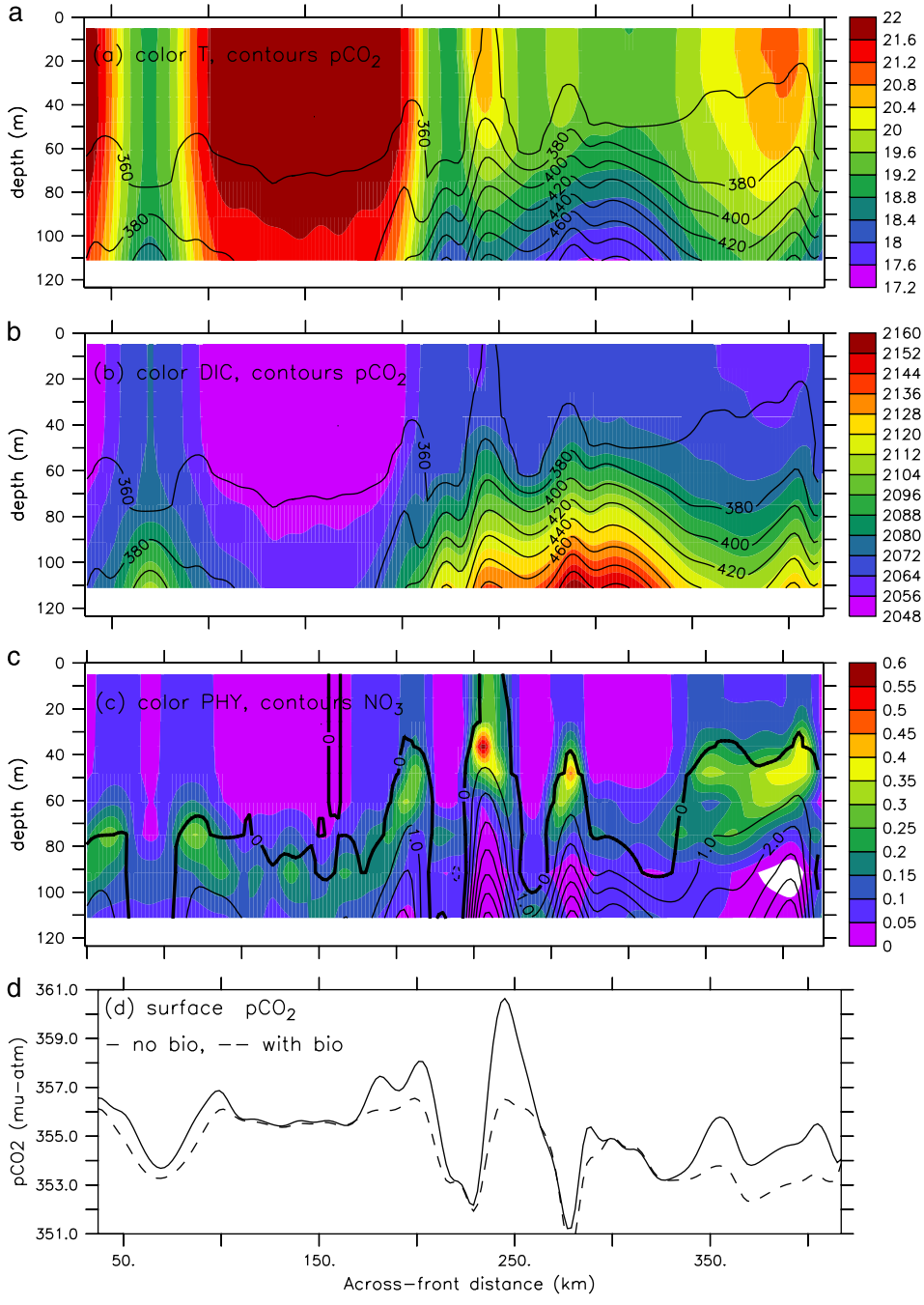

Figure 3. A north-south across-front section at x = 80 km (approximately mid-channel) showing (a) DIC and (b) temperature overlaid with contours of pCO_2 evaluated at atmospheric pressure. These fields are from day 30 of a model run initialized with $\gamma = 4$, $\gamma_s = 1$, constant ALK, and salinity, and forced with an east-west wind stress of 0.3 dyn cm^{-2}. The DIC is negatively correlated with T. There is no net heat flux and no biology in Figures 3a and 3b. DIC and cold water from the subsurface are upwelled and mixing vertically homogenizes the mixed layer conveying the upwelled water to the surface. When the wind stress is increased, the highs and lows in surface pCO_2 are more pronounced as increased mixing conveys a greater amount of upwelled DIC to the surface. (c) Phytoplankton concentration overlaid with contours of nitrate. Since nitrate is upwelled along with DIC, phytoplankton is concentrated at the sites of upwelling. It draws down the DIC and the pCO_2 as seen in Figure 3d in the regions where it had been elevated due to upwelling when there was no biology.

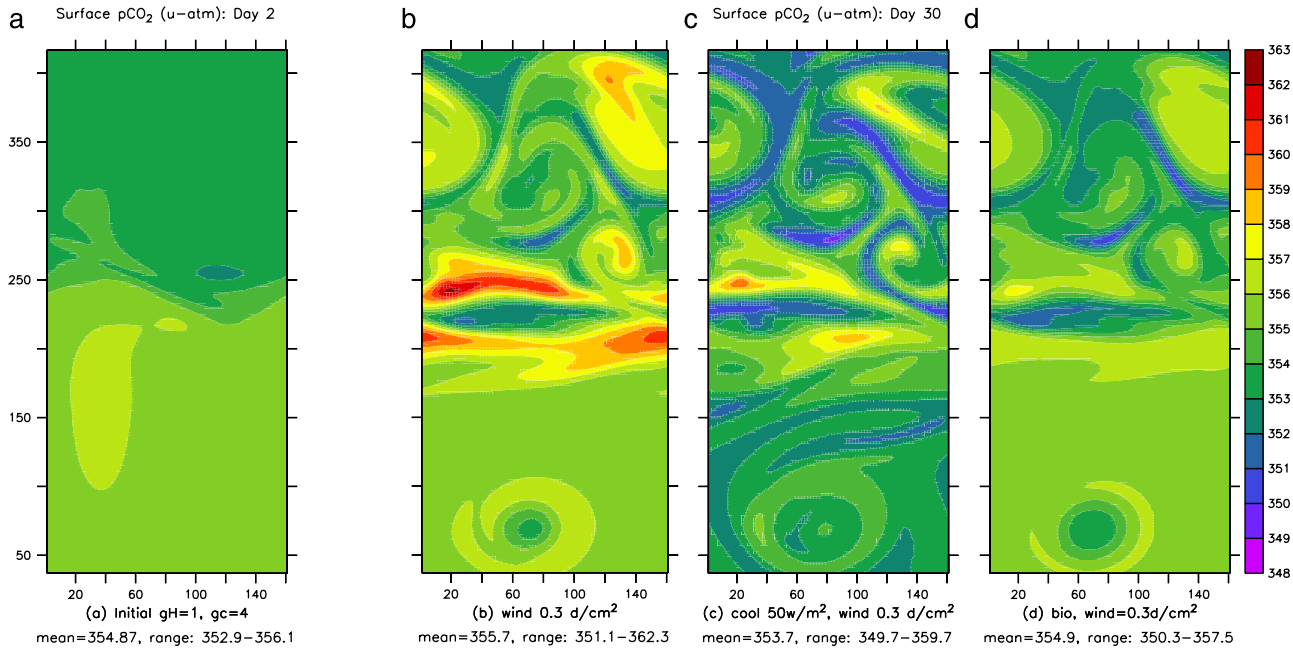

Figure 4. Surface pCO_2 in the model (a) on day 2, and (b)–(d) on day 30 of the simulation. These model runs were initialized with uniform pCO_2 at the surface and $\gamma = 4$ as shown in Figure 1. An east-west wind stress of 0.3 dyn cm^{-2} was applied at the surface. Figure 4b shows the localized increase in surface pCO_2 that results from the upwelling of DIC, though this is somewhat offset by the lowered temperature. Figure 4c shows a decrease in surface pCO_2 within certain regions when the surface is cooled by a heat loss of 50 watts m^{-2}. The reduction in pCO_2 is largest where the mixed layer depth is shallowest. Figure 4d shows the surface pCO_2 in a run with biological production that responds to the vertical flux of nitrate. The nitrate was initialized subsurface of 100 m using $\delta = 0.9$ which results in $\Gamma = 0.4$. The biological activity takes up most of the DIC upwelled and the pCO_2 enhancement seen in Figure 4b is no longer seen in Figure 4d. The range of pCO_2 variations is only 11, 10, and 7 μ-atm in each of these cases.

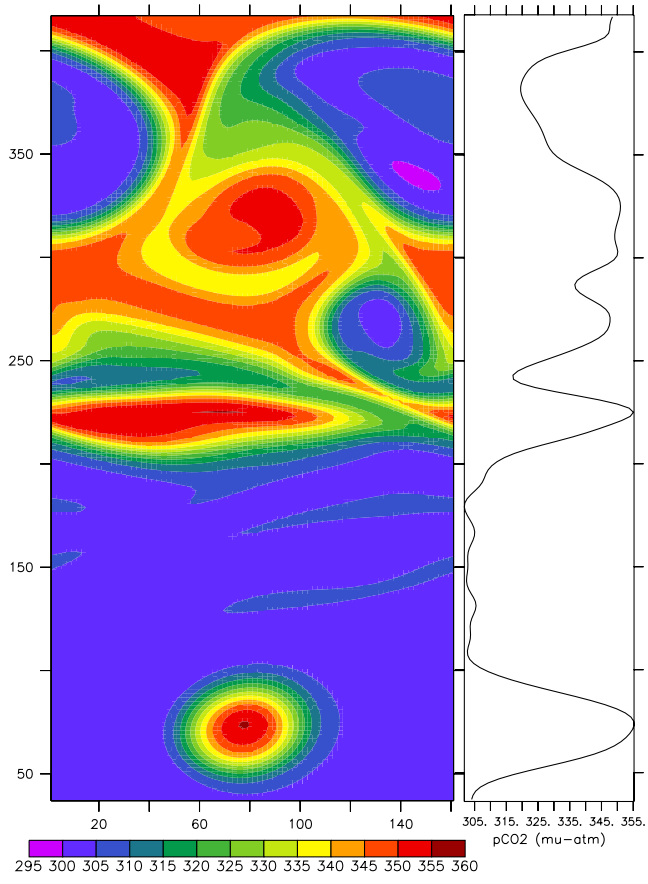

Figure 5. Surface pCO_2 on day 30 when the model is initialized with an across-front pCO_2 difference of approximately 60 μ-atm ($\gamma_s = 0.5$). The ratio of vertical DIC and T gradients is the same as in previous runs ($\gamma = 4$), but the effect of upwelling on the surface pCO_2 field is indiscernible since it is dominated by the horizontal stirring of the different pCO_2 waters. The color scale is different than in Figure 4. The variance in surface pCO_2 that initially exists at large scales is converted to smaller scales by horizontal advection as the flow evolves. The magnitude of the pCO_2 variations remains more or less unaltered. This model run was performed with a heat loss of 50 watts m^{-2}, but in general, the effect of cooling and biological productivity in response to submesoscale upwelling in undistinguishable in the surface pCO_2. The plot to the right shows the large surface pCO_2 variability along a mid-channel transect (at x = 80 km).